

## Effects of Preview on Human Control Behavior in Tracking Tasks With Various Controlled Elements

van der El, Kasper; Pool, Daan M.; van Paassen, Marinus M.; Mulder, Max

**DOI**

[10.1109/TCYB.2017.2686335](https://doi.org/10.1109/TCYB.2017.2686335)

**Publication date**

2018

**Document Version**

Accepted author manuscript

**Published in**

IEEE Transactions on Cybernetics

**Citation (APA)**

van der El, K., Pool, D. M., van Paassen, M. M., & Mulder, M. (2018). Effects of Preview on Human Control Behavior in Tracking Tasks With Various Controlled Elements. *IEEE Transactions on Cybernetics*, 48(4), 1242 - 1252. <https://doi.org/10.1109/TCYB.2017.2686335>

**Important note**

To cite this publication, please use the final published version (if applicable). Please check the document version above.

**Copyright**

Other than for strictly personal use, it is not permitted to download, forward or distribute the text or part of it, without the consent of the author(s) and/or copyright holder(s), unless the work is under an open content license such as Creative Commons.

**Takedown policy**

Please contact us and provide details if you believe this document breaches copyrights. We will remove access to the work immediately and investigate your claim.

# Effects of Preview on Human Control Behavior in Tracking Tasks with Various Controlled Elements

Kasper van der El, *Student Member, IEEE*, Daan M. Pool, *Member, IEEE*,  
Marinus (René) M. van Paassen, *Senior Member, IEEE*, and Max Mulder

**Abstract**—This paper investigates how humans use a previewed target trajectory for control in tracking tasks with various controlled element dynamics. The human’s hypothesized “near” and “far” control mechanisms are first analyzed offline in simulations with a quasi-linear model. Second, human control behavior is quantified by fitting the same model to measurements from a human-in-the-loop experiment, where subjects tracked identical target trajectories with a pursuit and a preview display, each with gain, single-, and double-integrator controlled element dynamics. Results show that target-tracking performance improves with preview, primarily due to the far-viewpoint response, which allows humans to cancel their own and the controlled element’s lags, without additional control activity. The near-viewpoint response yields better target tracking at higher frequencies, but requires substantially more control activity. The control-theoretic approach adopted in this paper provides unique quantitative insights into human use of preview, which can explain human behavior observed in other preview control tasks, like driving.

**Index Terms**—Human control models, man-machine systems, manual control, parameter estimation, preview control

## I. INTRODUCTION

**H**UMANS are highly effective adaptive controllers [1]. The seminal work of McRuer and his coworkers [2] shows that Human Controllers (HC) systematically adapt their control response to the dynamics of the Controlled Element (CE), the display type, and the characteristics of the target signal to be tracked. The HC’s adaptation mechanisms are relatively well-understood in simple error-compensation tasks [3]; however, few practical control tasks are purely compensatory. Instead, preview information of the target trajectory is often visible, commanding the HC were to steer to in the near future. Driving a car over a road is perhaps the best known example [4]–[6], but most vehicle control tasks involve preview, as well as many everyday motor control tasks [7], [8].

It has been shown that preview information helps HCs to improve task performance, compared to zero-preview (pursuit) tasks [5], [6], [9]–[11]. In tracking tasks, the amount of preview needed for maximum performance depends, at least, on the CE dynamics, and increases from about 0.5 to 1 s from position to acceleration control tasks [9]–[11]. To extrapolate these results to yet untested preview control tasks, many cybernetic models have been proposed (e.g., see [5], [6], [10]–[13]). Although several models accurately replicate the human’s control outputs, they are unsuitable to systematically study HC adaptation, because the proposed model inputs and

multiloop control dynamics were never shown to resemble those of the actual HC with objective measurements.

Recently, we measured the HC’s control dynamics in preview tracking tasks using a multiloop frequency-domain system identification technique [14]. Based on this, we extended McRuer *et al.*’s [2], [3] quasi-linear model for compensatory tracking tasks with two distinct responses that are based on a “near” and a “far” viewpoint on the previewed target ahead. The model’s physically interpretable parameters, like the viewpoints’ locations, can be explicitly estimated from measurement data. Thereby, this model may finally allow for quantifying HC control adaptation in preview tracking tasks, similar as established previously for compensatory tracking [1]–[3]. Unfortunately, the model’s near- and far-viewpoint responses are still poorly understood: while HCs always apply a far-viewpoint response, the presence of a near-viewpoint response appears to depend strongly on the tested subject and CE dynamics [14]. It is unclear when and why it is beneficial to respond to either one or two points on the previewed target ahead.

The goal of this paper is to explain how HCs use preview for control in manual tracking tasks with various CE dynamics. We first investigate the roles of the near- and far-viewpoint responses through offline simulations with the new preview model from [14], with gain, single-, and double-integrator CE dynamics. Second, we verify these offline predictions with measurements from a human-in-the-loop experiment, in which subjects performed a combined target-tracking and disturbance-rejection task with these same CEs, both in tasks with zero preview (i.e., pursuit) and 1 full second of preview. These experimental data were also used to derive the preview model in [14]; however, in this paper, we present a variety of new measures. Effects of preview are quantified with measures for tracking performance and control activity, and with estimates of input-to-error and open-loop dynamics. The HC’s underlying control behavior is investigated with non-parametric estimates of their multiloop response dynamics, and with estimates of the new preview model’s parameters [14].

This paper is structured as follows. In Section II, we summarize important aspects of HC behavior in preview tracking tasks, including the HC model from [14]. Offline model analyses are presented in Section III. The performed experiment and data analysis procedures are presented in Section IV, followed by the experimental results in Section V. We discuss these results and present our conclusions in the final two sections of this paper.

The authors are with the Control and Simulation section, Faculty of Aerospace Engineering, Delft University of Technology, 2629 HS Delft, The Netherlands. Corresponding author: K.vanderEl@tudelft.nl

## II. BACKGROUND

### A. The Control Task

The general layout of a combined target-tracking and disturbance-rejection control task is illustrated in Fig. 1. In these tasks, HCs are to minimize the tracking error:

$$e(t) = f_i(t) - x(t), \quad (1)$$

which is the difference between the current values of the target signal  $f_i(t)$  and the CE output  $x(t)$ . HCs generate control inputs  $u(t)$  to minimize this tracking error. At the same time, the CE is perturbed by disturbance signal  $f_d(t)$ , for which the HC must also compensate. In pursuit tasks, only the current target at time  $t$  is presented on the display, together with the CE output (see Fig. 2a). In preview tasks, an additional stretch of the future target  $f_i([t, t + \tau_p])$  is visible, up to preview time  $\tau_p$  s ahead (see Fig. 2b).

### B. Classical Approach and Results

HCs can adopt a multi-channel control organization in pursuit and preview tracking tasks, initiating an independent response to the target, the CE output, and the error, and in preview tasks also to the target ahead [2], [15]–[17]. Because explicit identification of all individual response dynamics is impossible [15], [17], HC behavior in these tasks has been traditionally analyzed by identifying lumped response dynamics [9], [11], [15], [17]. Ito & Ito [11], for example, measured the closed-loop dynamics from the target to the CE output:

$$H_{cl,t}(j\omega) = \frac{X(j\omega)}{F_i(j\omega)}, \quad (2)$$

with  $X$  and  $F_i$  the Fourier transforms of the respective signals. Perfect target-tracking is achieved when  $X(j\omega) = F_i(j\omega)$ , or equivalently, when  $|H_{cl,t}(j\omega)| = 1$  and  $\angle H_{cl,t}(j\omega) = 0$  deg. Ito & Ito's results (partly reproduced in Fig. 3) reveal that preview yields improved closed-loop characteristics, compared to the

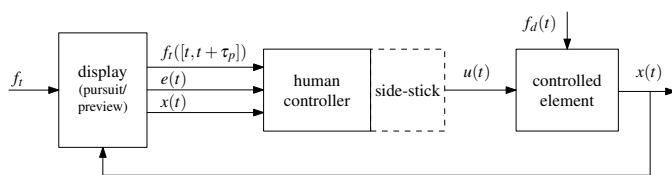


Fig. 1. The HC in a target-tracking and disturbance-rejection task.

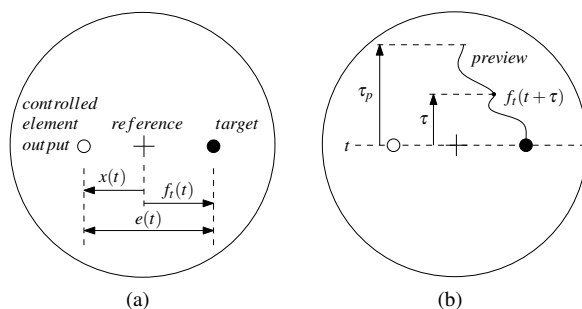


Fig. 2. Layout of the pursuit (a) and preview (b) displays.

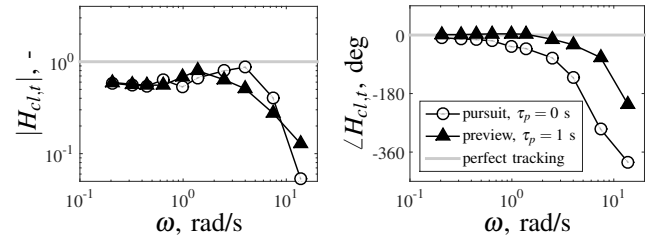


Fig. 3. Closed-loop dynamics in a double-integrator task with and without preview, average of two subjects (reproduced from [11]).

pursuit task, as the phase of  $H_{cl,t}(j\omega)$  is closer to zero. The closed-loop magnitude does not show a clear improvement. Preview thus primarily helps HCs to better synchronize the CE output with the target. In tasks with lower-order CE dynamics (e.g., a gain), HCs extend the region where the closed-loop phase approximates zero to higher frequencies [11]. Unfortunately, the (lumped) closed-loop dynamics obscure exactly how HCs use the available preview information, and also how they adapt their control response to the CE dynamics.

### C. Human Controller Model for Preview Tracking

Recently, we proposed a new model for pursuit and preview tracking tasks that separates the HC's responses to the different input signals [14]. Thereby, this model provides deeper insights in the human's underlying control mechanisms.

1) *The Model for Pursuit Tracking:* The HC model for pursuit tasks (see Fig. 4a) extends McRuer *et al.*'s simplified precision model for compensatory tracking [3]. The model is also quasi-linear, which means that linear describing functions account for the linear portion of the HC's response. Possible nonlinear and time-varying behavior are not explicitly modeled, nor are perception and motor noise; these are injected together as filtered white noise through the remnant  $n(t)$ .

The pursuit model involves a response to an error  $e^*(t)$ , with response dynamics  $H_{o_{e^*}}(j\omega)$  that are equal as in McRuer's simplified precision model [3], [14]:

$$H_{o_{e^*}}(j\omega) = K_{e^*} \frac{1 + T_{L,e^*} j\omega}{1 + T_{l,e^*} j\omega}. \quad (3)$$

$K_{e^*}$  is the error response gain and  $T_{L,e^*}$  and  $T_{l,e^*}$  are the lead and lag time constants, respectively. Similar as in compensatory tracking, HCs adapt to the CE dynamics by generating lead or lag in  $H_{o_{e^*}}(j\omega)$ , to establish a fair stretch of integrator-like dynamics around the open-loop crossover frequency ( $\omega_c$ ):  $|H_{o_{e^*}} H_{ce}| \approx \omega_c / j\omega$  [14], [15].

The error  $e^*(t)$ , a signal internal to the HC, is defined as the difference between the filtered target  $f_i^*$  and the CE output:

$$E^*(j\omega) = F_i^*(j\omega) - X(j\omega) = H_{o_f}(j\omega) F_i(j\omega) - X(j\omega). \quad (4)$$

In pursuit tasks,  $H_{o_f}(j\omega)$  was modeled as a simple gain,  $H_{o_f}(j\omega) = K_f$  [14]. When  $K_f = 1$ , (4) shows that  $e^*(t) = e(t)$ , hence that HCs respond to the true error and that they effectively exhibit a single-channel "compensatory" control organization [18]. A non-unity value of  $K_f$  implies a "pursuit" control organization [18], or the presence of a feedforward

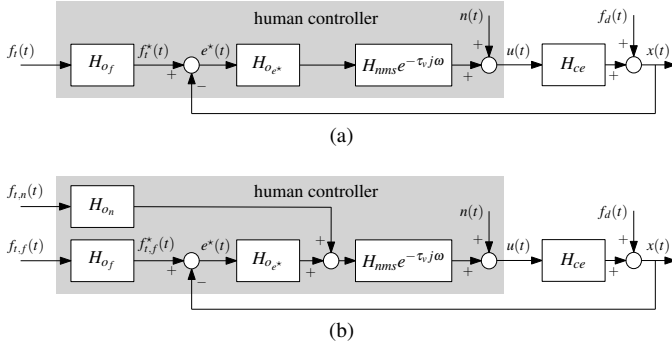


Fig. 4. Control diagrams of the HC model for pursuit (a) and preview (b) tracking tasks [14].

response. Higher values of  $K_f$  indicate a more aggressive response to the target, while  $K_f=0$  means that the HC completely ignores the target and focuses only on disturbance rejection. Single-subject data showed that  $K_f < 1$  for an (unstable) double integrator CE,  $K_f \approx 1$  for an integrator CE, and  $K_f > 1$  for a (stable) gain CE [14], which suggests that  $K_f$  reflects an important control-adaptation mechanism.

The model also incorporates the HC's most dominant physical limitations. Visual response delay  $\tau_v$  combines perceptual, cognitive and transport delays, and  $H_{nms}(j\omega)$  represents the combined neuromuscular system (NMS) and side-stick dynamics:

$$H_{nms}(j\omega) = \frac{\omega_{nms}^2}{(j\omega)^2 + 2\zeta_{nms}\omega_{nms}j\omega + \omega_{nms}^2}, \quad (5)$$

with  $\omega_{nms}$  and  $\zeta_{nms}$  the natural frequency and damping ratio.

2) *The Model for Preview Tracking*: Fig. 4b shows the HC model for preview tasks, which extends the pursuit model. Two responses, each initiated with respect to a different viewpoint, can capture the HC's response to the entire previewed target [14]. A far viewpoint  $f_{i,f}(t)$  feeds the "pursuit" control-loop, while an additive, parallel feedforward channel describes the HC's response to a near viewpoint  $f_{i,n}(t)$ . The near- and far-viewpoints are located  $\tau_n$  and  $\tau_f$  s ahead on the previewed target:

$$f_{i,n}(t) = f_i(t + \tau_n), \quad f_{i,f}(t) = f_i(t + \tau_f). \quad (6)$$

As the HC can select which points to respond to, based on the task specifics, both  $\tau_n$  and  $\tau_f$  are free model parameters. Note that these viewpoints do not necessarily correspond to the two levels, or points, used in many driver models (e.g., [19], [20]).

In preview tracking tasks, HCs were found to smooth the target in the far viewpoint, so  $H_{o_f}(j\omega)$  includes a low-pass filter [14]:

$$H_{o_f}(j\omega) = K_f \frac{1}{1 + T_{l,f}j\omega}. \quad (7)$$

The far-viewpoint response thus only describes low-frequency target-tracking behavior, with the reciprocal of the time constant  $T_{l,f}$  as cut-off frequency. The HC's response to higher frequencies in the target signal was modeled as an open-loop response  $H_{o_n}(j\omega)$  with respect to the near viewpoint [14]:

$$H_{o_n}(j\omega) = K_n \frac{j\omega}{1 + T_{l,n}j\omega}, \quad (8)$$

with gain  $K_n$  and high-pass filter time-constant  $T_{l,n}$ . The limited data provided in [14] suggests that not all subjects apply a near-viewpoint response in tasks with single- and double-integrator CE dynamics.

### III. OFFLINE MODEL ANALYSIS

The exact roles of the near- and far-viewpoint responses are not yet fully understood. To gain more insight, we mathematically derive the HC dynamics that result in "perfect" target-tracking, and we investigate the contributions of both responses with model simulations.

#### A. Perfect Target-Tracking

The introduced HC model (Fig. 4) can be restructured into the mathematically equivalent two-channel model of Fig. 5 (see [14]). Here, the HC is modeled to respond to the target and the CE output, with lumped dynamics  $H_{o_t}(j\omega)$  and  $H_{o_x}(j\omega)$ :

$$H_{o_t} = [H_{o_f}H_{o_e^*}e^{\tau_f j\omega} + H_{o_n}e^{\tau_n j\omega}]H_{nms}e^{-\tau_v j\omega}, \quad (9)$$

$$H_{o_x} = H_{o_e^*}H_{nms}e^{-\tau_v j\omega}. \quad (10)$$

In (9) and (10) the dependency on  $j\omega$  is left out for better readability. Using Fig. 5, the target closed-loop can be written as

$$H_{cl,t}(j\omega) = \frac{X(j\omega)}{F_t(j\omega)} = \frac{H_{o_t}(j\omega)H_{c_e}(j\omega)}{1 + H_{o_x}(j\omega)H_{c_e}(j\omega)}. \quad (11)$$

Substituting  $X(j\omega)/F_t(j\omega)=1$  (i.e., perfect target-tracking), and solving for  $H_{o_t}(j\omega)$ , yields the perfect target-tracking dynamics  $H_{o_t}^P(j\omega)$ :

$$H_{o_t}^P(j\omega) = H_{o_x}(j\omega) + \frac{1}{H_{c_e}(j\omega)}. \quad (12)$$

Because the form of the response function  $H_{o_x}(j\omega)$  is identical in tasks with and without preview for a given CE [14], the form of  $H_{o_t}^P(j\omega)$  is also fixed. For example,  $H_{o_x}(j\omega)$  is approximately a gain for integrator CE dynamics.  $1/H_{c_e}(j\omega)$  is then a pure differentiator, which has a negligible magnitude at low frequencies, but a much higher magnitude than  $H_{o_x}(j\omega)$  at high frequencies.  $H_{o_t}^P(j\omega)$  is thus dictated by  $H_{o_x}(j\omega)$  at low frequencies and by  $1/H_{c_e}(j\omega)$  at high frequencies. The modeled HC target response in (9) has a similar form; for integrator CE dynamics, it is dictated by gain  $K_f K_{e^*}$  at low frequencies and by differentiator  $K_n j\omega$  at higher frequencies. This suggests that HCs attempt to approach perfect target-tracking when preview is available.

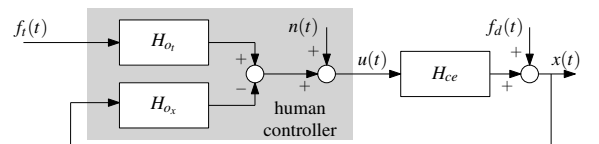


Fig. 5. Two-channel control diagram of the HC.

## B. Model Simulations

Two key aspects of the model are essential for the difference between pursuit and preview tasks: 1) the point on the target ahead that is the input to the HC's "pursuit" response (characterized by  $\tau_f$ ), and 2) the presence and strength of the additive open-loop near-viewpoint response (characterized mostly by  $K_n$ , but to a lesser extent also by the other model parameters). Next, we investigate these two aspects for gain, single-, and double-integrator CE dynamics.

1) *Settings*: For tasks with 0 and 1 s of preview, estimated model parameters (single-subject data) are reproduced from [14] in Table I; these are used as baseline in the simulations. The used target ( $\sigma_{f_i}=0.5$  inch) and disturbance ( $\sigma_{f_d}=0.2$  inch) signals are each the sum of 20 sines, with a square amplitude spectrum (1.5 rad/s bandwidth), augmented with a high-frequency shelf where the amplitudes are attenuated (see [14] for details). No remnant is included.

2) *Analysis of the Far-Viewpoint Location*: We step-wise increase the value of  $\tau_f$  from 0 s (i.e., pursuit tracking) to 1.5 s, while keeping all other parameters fixed at the pursuit settings in Table I. Fig. 6a shows that the variance of the tracking error reduces substantially when  $\tau_f$  increases, for all CE dynamics. Doing so, the target response exhibits phase lead that compensates for the CE's inherent lag, and the HC's NMS lag and visual response delay. The phase becomes markedly closer to  $H_{o_t}^P(j\omega)$ , especially at mid-frequencies, as shown for integrator CE dynamics in Fig. 6e. Responding to the target ahead requires no additional control activity (constant  $\sigma_u^2$  in Fig. 6a), because a pure delay like  $\tau_f$  only affects the phase of the target response (all  $|H_{o_t}(j\omega)|$  lines overlap in Fig. 6c). Fig. 6a also shows that it is beneficial to respond to the target farther ahead for higher-order CEs, to compensate for its larger inherent lag.

3) *Analysis of the Near-Viewpoint Response*: We step-wise increase the value of  $K_n$  from 0 and 0.6, keeping all other parameters fixed at the preview settings in Table I. Fig. 6b shows that only a small performance improvement is possible by increasing  $K_n$ , which comes at the cost of a substantially

higher control activity. For some subjects no near-viewpoint response was found in [14]; possibly, these subjects aimed for lower control activity, instead of slightly better performance. The Bode plots (Fig. 6 d and f) show that an additional near-viewpoint response mainly affects the high frequencies of  $H_{o_t}(j\omega)$ , which resembles  $H_{o_t}^P(j\omega)$  better in both magnitude and phase if  $K_n$  is non-zero. In particular, the characteristic increasing phase lead that results from responding to a far viewpoint (due to negative delay  $\tau_f$ ) disappears, even with low values of  $K_n$ .

4) *Analysis of Time-Traces*: The simulated CE output is calculated with (11) for both the pursuit and preview parameters in Table I, with the disturbance set to zero. Fig. 7 shows that the CE output follows the target signal much better with preview, lagging less behind, which is consistent with Fig. 6. Still, the fast oscillations, or high frequencies, are not completely reproduced; the CE output often remains on the inside of the target signal "corners", reflecting corner-cutting behavior. This corresponds well with  $|H_{o_t}(j\omega)|$  at high frequencies (Fig. 6d), which is smaller than than required for perfect target-tracking when  $K_n$  is small. With double integrator CE dynamics the target's high frequencies are hardly

TABLE I  
TESTED CONDITIONS AND MODEL PARAMETERS (SINGLE-SUBJECT DATA),  
ADAPTED FROM [14].

$H_{ce}$	$K_{ce}$		$K_{ce}/s$		$K_{ce}/s^2$	
$K_{ce}, -$	0.8	1.5	5	5	5	5
$\tau_p, s$	0	1	0	1	0	1
abbreviation	GN0	GN1	SI0	SI1	DI0	DI1
$K_{e^*}, -$	3.85	6.62	1.43	1.11	0.14	0.14
$T_{l,e^*}, s$	2.06	2.39	-	-	-	-
$T_{l,e^*}, s$	-	-	-	-	2.54	2.22
$\tau_v, s$	0.18	0.16	0.23	0.18	0.28	0.31
$\omega_{nms}, rad/s$	17.9	18.0	11.2	10.2	6.15	5.33
$\zeta_{nms}, -$	0.18	0.37	0.30	0.26	0.67	0.50
$K_n, -$	-	0.06	-	0.18	-	0.32
$\tau_n, s$	-	0.08	-	0.34	-	0.00
$T_{l,n}, s$	-	0.06	-	0.04	-	5.89
$K_f, -$	1.21	1.11	0.95	1.12	0.54	0.63
$\tau_f, s$	-	0.55	-	0.70	-	0.99
$T_{l,f}, s$	-	0.26	-	0.38	-	0.59

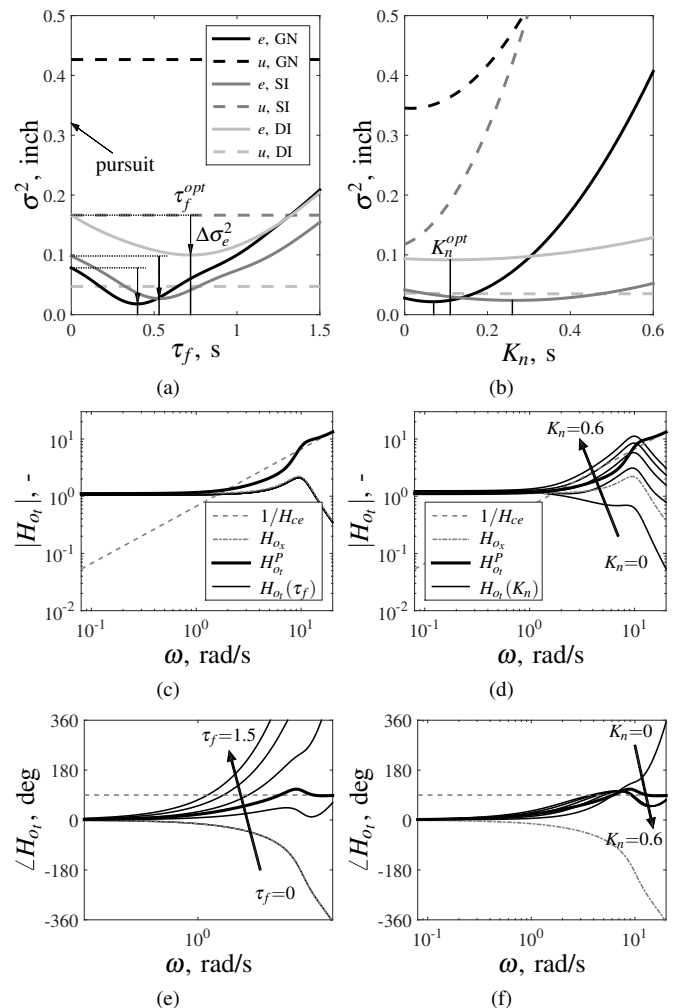


Fig. 6. Simulated effects of  $\tau_f$  (a), (c), and (e), and  $K_n$  (b), (d), and (f); Bode plots (c-f) show only integrator CE dynamics results.

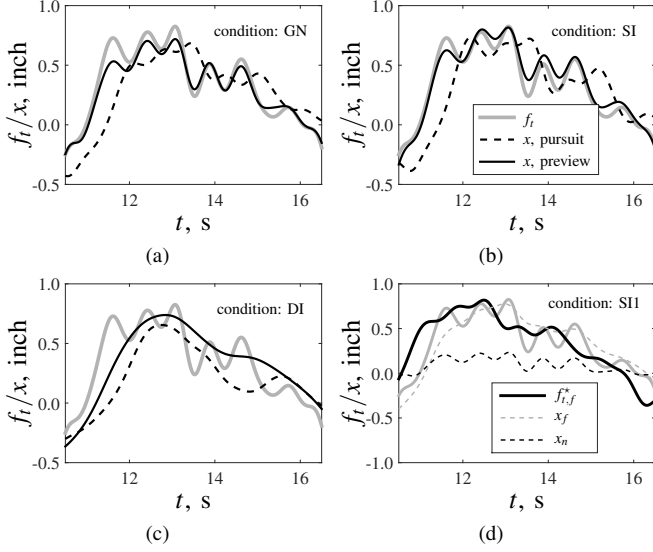


Fig. 7. Simulated time-traces of the CE output: the benefit of preview (a-c), and the contributions of the near- and far-viewpoint responses (d).

tracked at all (Fig. 7c).

Fig. 7d shows the contributions of the near- and far-viewpoint responses when tracking with preview and integrator CE dynamics. The near-viewpoint response accounts for an output ( $X_n = H_{o_n} H_{nms} e^{-\tau_n} F_{t,n}$ ) that is identical to the high-frequency sinusoids in the target signal. The filtered far-viewpoint ( $F_{t,f}^* = H_{o_f} F_{t,f}$ ) lacks exactly these high frequencies; tracking it results in an output ( $X_f$ , obtained from closed-loop simulation with  $K_n$ ,  $\tau_n$  and  $T_{l,n}$  all set to zero) that approximates the target signal's low frequencies.

#### IV. METHOD

Next, the model simulations are verified with experimental data. Details of the experiment and the data analysis procedures are presented in this section.

##### A. The Experiment

Twelve subjects performed a combined target-tracking and disturbance-rejection tasks. Two independent variables were varied, the display and the CE dynamics. The display (see Fig. 2) showed either 0 (i.e., pursuit) or 1 s of preview; the CE had gain, integrator, or double integrator dynamics. All subjects performed the full factorial of the two independent variables in a randomized order. The six experimental conditions are summarized in Table I; full details of the experimental settings, procedure, and apparatus are given in [14].

##### B. Data Analysis

1) *Error and Control Output Variance*: The variances of the tracking error and the control output are used as measures for the achieved tracking performance and the applied control activity, respectively. The individual contributions due to the target, disturbance, and HC remnant are estimated by integrating the error and control output auto spectral-density functions only over the respective signal's input frequencies [21].

2) *Input-to-Error Dynamics*: The target-to-error and disturbance-to-error dynamics,  $H_{f_t,e}(j\omega_t)$  and  $H_{f_d,e}(j\omega_d)$ , respectively, quantify the error amplification/attenuation, relative to the respective input signal, in the frequency domain. Both are estimated at the input signal's frequencies,  $\omega_t$  or  $\omega_d$ , as follows:

$$H_{f_t,e}(j\omega_t) = \frac{E(j\omega_t)}{F_t(j\omega_t)}, \quad H_{f_d,e}(j\omega_d) = \frac{E(j\omega_d)}{F_d(j\omega_d)}. \quad (13)$$

3) *Open-Loop Dynamics*: In the frequency domain, performance and stability are characterized by the open-loop crossover frequency  $\omega_c$  and phase margin  $\phi_m$ , respectively. In a combined target-tracking and disturbance-rejection task, two open-loop dynamics can be formulated,  $H_{ol,t}(j\omega)$  and  $H_{ol,d}(j\omega)$  [21]:

$$\begin{aligned} H_{ol,t}(j\omega_t) &= \frac{X(j\omega_t)}{E(j\omega_t)} \\ &= \frac{H_{o_t}(j\omega_t)H_{ce}(j\omega_t)}{1 + [H_{o_x}(j\omega_t) - H_{o_t}(j\omega_t)]H_{ce}(j\omega_t)}, \quad (14) \\ H_{ol,d}(j\omega_d) &= -\frac{X(j\omega_d) - F_d(j\omega_d)}{X(j\omega_d)} \\ &= H_{ce}(j\omega_d)H_{o_x}(j\omega_d). \quad (15) \end{aligned}$$

Crossover occurs at the frequency  $\omega_c$  for which  $|H_{ol}(j\omega)|=1$ , the corresponding phase margin  $\phi_m$  is  $180 + \angle H_{ol}(j\omega_c)$  deg.

4) *Non-Parametric Multiloop System Identification*: Non-parametric estimates of  $H_{o_t}(j\omega)$  and  $H_{o_x}(j\omega)$  in Fig. 5 are used to objectively quantify the HC's multiloop control dynamics. Both responses can be estimated simultaneously with a system identification method based on Fourier coefficients [14], [22], [23]. From Fig. 5 it follows that the modeled control output is

$$U(j\omega) = H_{o_t}(j\omega)F_t(j\omega) - H_{o_x}(j\omega)X(j\omega) + N(j\omega). \quad (16)$$

Two equations, needed to solve for the two unknown dynamics, are obtained by evaluating (16) both at the input frequencies  $\omega_t$  of target signal, and by interpolating the signals  $F_t$ ,  $X$ , and  $U$  in the frequency domain from the disturbance frequencies  $\omega_d$  to these same  $\omega_t$  (yielding  $\tilde{F}_t$ ,  $\tilde{X}$ , and  $\tilde{U}$ ). Assuming zero remnant, it follows that

$$\begin{bmatrix} U(j\omega_t) \\ \tilde{U}(j\omega_t) \end{bmatrix} = \begin{bmatrix} F_t(j\omega_t) & -X(j\omega_t) \\ \tilde{F}_t(j\omega_t) & -\tilde{X}(j\omega_t) \end{bmatrix} \begin{bmatrix} H_{o_t}(j\omega_t) \\ H_{o_x}(j\omega_t) \end{bmatrix}. \quad (17)$$

Eq. (17) can be solved for  $H_{o_t}(j\omega_t)$  and  $H_{o_x}(j\omega_t)$ . Similarly, estimates can be obtained at the disturbance signal input frequencies, by evaluating (17) at  $\omega_d$ , after interpolating from  $\omega_t$  to  $\omega_d$ .

5) *Model Parameter Estimation*: Estimates of the model parameters are used to explicitly quantify human control behavior, including the characteristics of the near- and far-viewpoint responses. The model parameters are estimated by minimizing a least-squares cost function  $J$ , which is based on a frequency-domain error  $E_u$  between the measured and modeled control outputs  $U$  and  $\hat{U}$ , respectively:

$$E_u(j\omega|\Theta) = U(j\omega) - \hat{U}(j\omega|\Theta), \quad (18)$$

$$J(\Theta) = \sum_{l=1}^{N_l} \left| E_u(j\omega_l|\Theta) \right|^2. \quad (19)$$

$N_l$  is the number of measured frequencies below a chosen cut-off frequency, here 25 rad/s. The five-run frequency-domain average of the measured control output signals is used to reduce effects of the remnant on the parameter estimates. The modeled control output is obtained from (16) with remnant  $N$  set to zero. The parameter vector  $\Theta$  is  $[K_{e^*} T_{l,e^*} T_{L,e^*} \tau_v \omega_{nms} \zeta_{nms} K_f \tau_f T_{l,f} K_n \tau_n]^T$ . Because the break frequency of the near-viewpoint high-pass filter was generally well above measured frequency range in [14],  $T_{l,n}$  is removed from the model here, such that (8) simplifies to a pure differentiator. NMS natural frequencies above the highest input frequency (about 15 rad/s) cannot be estimated accurately, for subjects where this applies we fix  $\omega_{nms}$  at 15 rad/s. A Nelder-Mead simplex algorithm is used to minimize  $J$ , constrained only to avoid solutions that contain negative parameters. The best solution is selected from 100 randomly initialized optimizations.

6) *Data Processing*: All non-parametric measures are calculated per run, and then averaged over the five measurement runs. Crossover frequencies and phase margins are calculated from the fitted HC model, which allows for better estimates of crossover frequencies outside the range of input frequencies. A repeated-measures two-way ANOVA is applied to test for significant differences in performance and control activity, crossover frequency, and phase margin; results are compensated with a conservative Greenhouse-Geisser correction when the assumption of sphericity is violated. Errorbars on the results in the next section represent 95% confidence intervals, corrected for between-subject variability.

### C. Hypotheses

Preview is information about the future target signal, so we expect that it affects only the target-tracking, and not the disturbance-rejection part of the task. This leads to the following hypotheses:

- I: Target-tracking performance improves with preview, in accordance with [9]–[11] and our offline model predictions; this will manifest in a lower error variance at the target frequencies and higher target crossover frequencies and phase margins;
- II: Disturbance-rejection behavior is similar in pursuit and preview conditions, resulting in similar control output variances and  $H_{o_x}(j\omega)$  dynamics, hence similar parameters  $K_{e^*}$ ,  $T_{l,e^*}$ ,  $T_{L,e^*}$ ,  $\tau_v$ ,  $\omega_{nms}$ , and  $\zeta_{nms}$ .

Based on our offline model analyses (Section III-B) we further hypothesize that:

- III: Subjects respond to the target ahead to improve performance (characterized by  $\tau_n$  and  $\tau_f$ ); furthermore, the two viewpoints are farther ahead in conditions with higher-order CE dynamics, to generate more compensating phase lead for the CE's larger inherent phase lag;
- IV: Subjects initiate a weak near-viewpoint response, reflected by a small but non-zero value of  $K_n$ , to better match the phase required for perfect target-tracking, without substantially increasing control activity.

## V. RESULTS

### A. Tracking Performance and Control Activity

Fig. 8a shows that tracking performance is substantially better (lower  $\sigma_e^2$ ) in conditions with preview, which corresponds to results in [9]–[11]. Especially target-tracking performance improves (gray part of the bars), but the slight performance increase due to reduced HC remnant is also significant (see Table II). Neither disturbance-rejection performance, nor control activity (Fig. 8b), are significantly different with preview. Fig. 8 also shows that the performance improvement predicted by the model simulations in Section III-B matches reasonably well with the experimental results.

With higher-order CE dynamics, tracking performance is substantially worse (Fig. 8a). However, this effect is smaller when preview is available, especially at the target and remnant frequencies (significant interaction effects). Increasing the order of the CE dynamics markedly affects the control activity distribution: the target component decreases significantly, while the remnant component increases significantly.

The estimated input-to-error dynamics are shown in Fig. 9 for integrator CE dynamics. The characteristic error-amplification peak, caused by the HC's response time-delay [3], is clearly present in disturbance rejection, both with and without preview (indicated by  $|H_{f_d,e}| > 1$  in Fig. 9b). In target tracking (Fig. 9a) this peak is only visible in pursuit

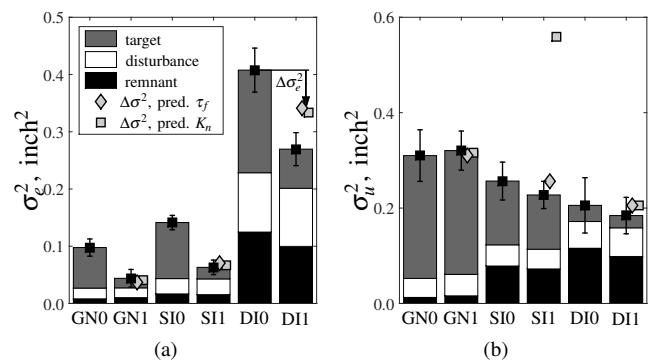


Fig. 8. Variances of the tracking error (a) and the control output (b).

TABLE II  
ERROR AND CONTROL OUTPUT ANOVA RESULTS.<sup>1</sup>

		error, $e$			control output, $u$		
		df	F	sig.	df	F	sig.
$\sigma_e^2$	display	(1,11)	127	**	(1,11)	1.31	-
	dynamics	(1.07,11.8)	213	**	(1.23,13.6)	8.4	**
	disp.*dyn.	(1.05,11.5)	13.5	**	(2,22)	0.91	-
$\sigma_f^2$	display	(1,11)	305	**	(1,11)	1.44	-
	dynamics	(1.16,12.8)	83.3	**	(2,22)	197	**
	disp.*dyn.	(1.11,12.3)	14.5	**	(2,22)	0.95	-
$\sigma_d^2$	display	(1,11)	0.22	-	(1,11)	0.81	-
	dynamics	(1.01,11.1)	138	**	(1.08,11.9)	2.30	-
	disp.*dyn.	(1.03,11.3)	0.20	-	(1.36,15.0)	0.79	-
$\sigma_r^2$	display	(1,11)	1.43	*	(1,11)	1.34	-
	dynamics	(1.03,11.3)	135	**	(1.16,12.7)	14.2	**
	disp.*dyn.	(1.08,11.8)	7.98	*	(2,22)	1.10	-

<sup>1</sup> Symbols \*\*, \*, and - indicate highly significant ( $p < .01$ ), significant ( $p < .05$ ), and non-significant ( $p > .05$ ) results, respectively.

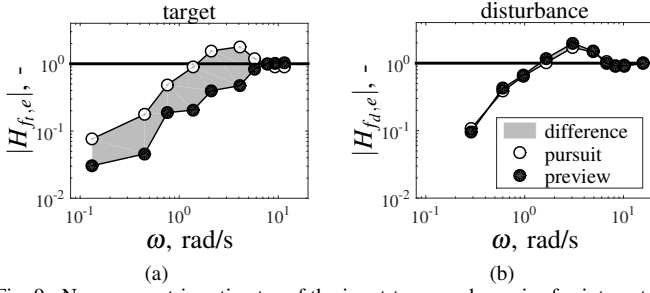


Fig. 9. Non-parametric estimates of the input-to-error dynamics for integrator CE conditions, single-subject data.

tasks. With preview,  $|H_{f_i, e}|$  is always smaller than one, so the error is attenuated all input frequencies. This is evidence that preview enables HCs to compensate for their own response delays.

### B. Open-Loop Dynamics

In pursuit conditions, the measured target open-loop dynamics (Fig. 10, gray markers/line) resemble an integrator with a time delay around crossover, in accordance with [15], [24]. For double integrator CE dynamics subjects managed to generate integrator magnitude characteristics in only a minor region around crossover, due to the difficulty of this condition. All disturbance open-loop dynamics (not shown) have a similar shape, both in pursuit and preview conditions. With the introduction of preview, the magnitude of the target open-loop dynamics increases below the crossover frequency, and then drops off with a slope larger than that of an integrator

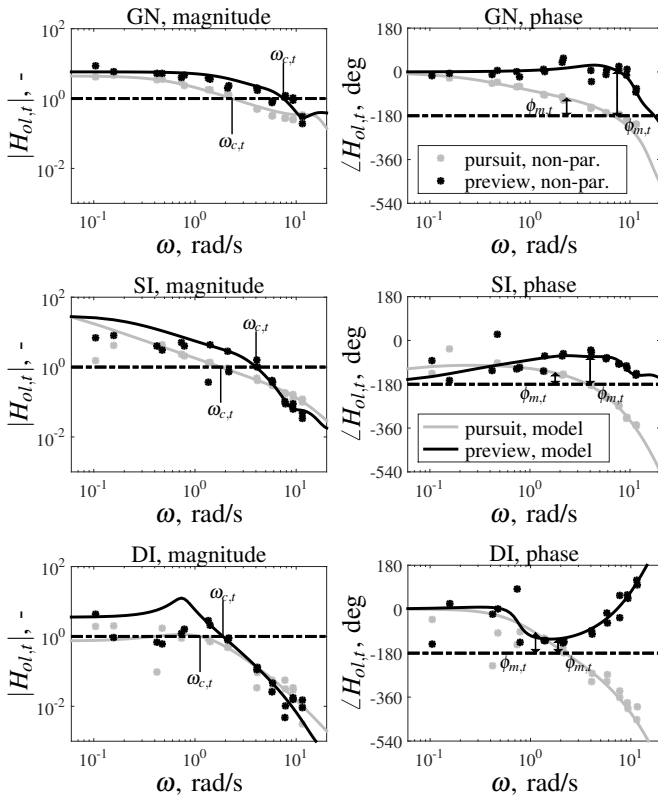


Fig. 10. Target open-loop dynamics, single-subject data.

(black markers/line, Fig. 10); additionally, the characteristic pure delay is not visible in the open-loop phase.

The target crossover frequency (Fig. 11a) and phase margin (Fig. 11c) are both higher in conditions with preview (significant effect, Table III), pointing to improved target-tracking performance and stability. The average target phase margins are between the values predicted by the near- and far-viewpoint model simulations (Section III-B), suggesting that a combination of both responses is active (except in double integrator tasks). Note that the measured crossover frequencies are slightly lower than the idealized predictions. The disturbance crossover frequency (Fig. 11b) and phase margin (Fig. 11d) are similar in pursuit and preview conditions. Only for gain CE dynamics the disturbance crossover frequency is slightly lower with preview, yielding a significant display effect; however, this crossover frequency was difficult to estimate, due to the relatively low control activity at disturbance frequencies in gain CE conditions (see Fig. 8b).

The measured crossover frequencies (except target tracking with preview) are relatively low: they are in the region where crossover regression occurs in compensatory tracking tasks ( $0.8\omega_c < \omega_i$  [2], [25]), as illustrated in Fig. 11. Little is

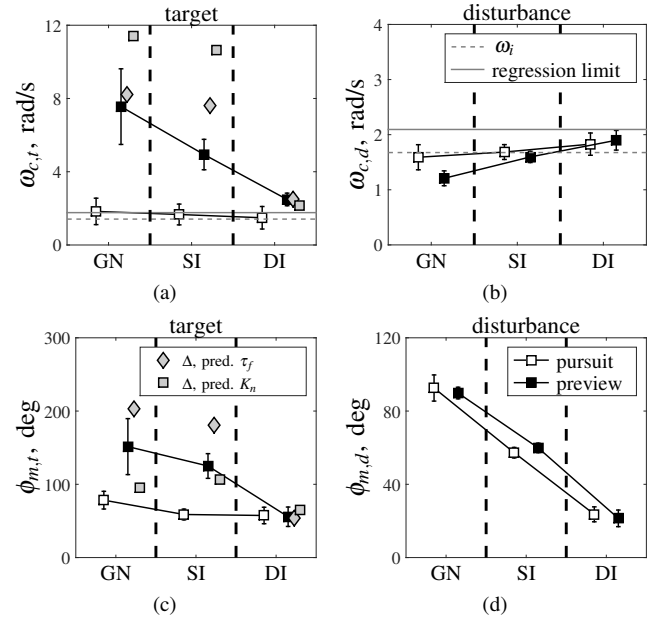


Fig. 11. Crossover frequencies (a,b) and phase margins (c,d).

TABLE III  
CROSSOVER FREQUENCY AND PHASE MARGIN ANOVA RESULTS.<sup>1</sup>

	target			disturbance		
	df	F	sig.	df	F	sig.
$\omega_c$ display	(1,11)	35.7	**	(1,11)	7.80	*
dynamics	(1.20,13.2)	19.7	**	(1.27,14.0)	8.35	**
disp.*dyn.	(1.23,13.5)	12.1	**	(2,22)	8.69	**
$\phi_m$ display	(1,11)	37.7	**	(1,11)	0.41	-
dynamics	(1.58,17.4)	19.9	**	(1.20,13.1)	316	**
disp.*dyn.	(1.17,12.9)	8.32	**	(1.33,14.7)	1.40	-

<sup>1</sup> Symbols \*\*, \*, and - indicate highly significant ( $p < .01$ ), significant ( $p < .05$ ), and non-significant ( $p > .05$ ) results, respectively.

known of this phenomenon in pursuit and preview tasks. The relative invariance of these low crossover frequencies with CE dynamics was reported earlier in similar pursuit tracking tasks [15], [26].

### C. Human Multiloop Control Dynamics

Fig. 12 shows Bode plots of the estimated  $H_{o_r}(j\omega)$  and  $H_{o_x}(j\omega)$ . As shown before in [14], the model fits (solid lines) coincide well with the non-parametric identification results (markers). Note that a similar equalization is visible as in compensatory tracking tasks [3]; both  $H_{o_r}(j\omega)$  and  $H_{o_x}(j\omega)$  exhibit a -1, 0, and +1 mid-frequency magnitude slope for gain, single-, and double-integrator CE dynamics, respectively.

The target response in pursuit conditions (as well as the CE output response in all conditions), shows the characteristic high-frequency phase roll-off caused by the HC's response delay and NMS lags. In the preview conditions such phase lag is not present in  $H_{o_r}(j\omega)$ ; instead, phase lead is generated, similar as in the simulations in Section III-B. The resulting phase characteristics resemble perfect target-tracking much better, so subjects clearly apply control actions that cancel most of the lag from their own response and the CE dynamics. At higher frequencies and for higher-order CE dynamics the perfect target-tracking phase is matched less well.

Fig. 12 also shows that the target response high-frequency magnitude is lower than that required for perfect target-tracking. This indicates corner-cutting behavior, and corresponds to the model simulations with low values of the near-viewpoint gain  $K_n$  (Section III-B).

### D. Model Parameters

1) *Internal-Error Response*: In gain CE conditions, both  $K_{e^*}$  and  $T_{l,e^*}$  increase slightly with preview (Fig. 13). As a result, the total error-response dynamics have a higher magnitude at the lowest frequencies, but remain similar over most of the measured frequency range. Similarly, preview yields a slightly higher  $K_{e^*}$  and  $T_{l,e^*}$  in double integrator conditions, which also points to a higher low-frequency magnitude. For integrator CE tasks,  $K_{e^*}$  is identical with and without preview.

2) *Physical Limitations*:  $\tau_v$ ,  $\omega_{nms}$ , and  $\zeta_{nms}$  (Fig. 13) are not systematically adapted when preview becomes available. Only the NMS damping  $\zeta_{nms}$  appears to be slightly lower with preview. Increasing the order of the CE dynamics yields more pronounced effects: the visual-response delay  $\tau_v$  increases, while the NMS bandwidth ( $\omega_{nms}$ ) decreases; such adaptations have been measured before in [2], [15], [24], [26].

3) *Far-Viewpoint Response*: Fig. 14 shows the estimated far-viewpoint parameters.  $\tau_f$  is larger for higher-order CE dynamics, indicating that subjects respond to the target farther ahead, to generate more compensating phase lead. For double integrator CE dynamics,  $\tau_f$  is approximately at the limit of the presented preview (1 s), suggesting that the tracking performance in this condition may further improve with more preview. The far-viewpoint filter time-constant  $T_{l,f}$  is also larger for higher-order CEs, such that less of the target's high frequencies are tracked through the far-viewpoint response. To compensate for the phase lag introduced by the low-pass

filter, the measured values of  $\tau_f$  are consistently higher than predicted in Section III-B, where this low-pass filter was not considered (i.e.,  $T_{l,f}=0$ ).

For gain and integrator CE dynamics, the target weighting gain  $K_f$  is similar in pursuit and preview conditions. For double integrator CE dynamics,  $K_f$  is much larger with preview, indicating that subjects are responding more aggressive to the target signal. The difficulty of the pursuit task with double integrator CE dynamics likely forced subjects to prioritize stabilizing the CE's output, so less effort was put in target tracking. This is consistent with the generally lower values of  $K_f$  with higher-order CEs, and also with the lower control activity at the target frequencies (Fig. 8).

4) *Near-Viewpoint Response*: Fig. 15 shows the estimated near-viewpoint parameters.  $K_n$  is small but always non-zero, suggesting that most subjects initiated a near-viewpoint response; however, this does not correspond to the Bode plots in Fig. 12. For example, for double integrator CE dynamics the increasing high-frequency phase of  $H_{o_r}(j\omega)$  suggests that no near-viewpoint response is present, while  $K_n$  is estimated at 0.05. For single integrator CE dynamics, the phase flattening of  $H_{o_r}(j\omega)$  at high frequencies does suggest that a near-viewpoint response is initiated, while  $K_n$  is estimated at 0.08. It is thus difficult to determine whether a subject initiated a near-viewpoint response, or not, merely from  $K_n$ . The adaptation of  $K_n$  to the CE dynamics is similar as predicted by the model simulations (Section III-B), with the highest value of  $K_n$  found in single integrator conditions. As the estimated values of  $K_n$  are lower than predicted, it appears that subjects prioritize a low control activity over enhanced performance.

$\tau_n$  is larger for higher-order CE dynamics, similar as  $\tau_f$ . However, between-subject variations are large, especially for double integrator CE dynamics. Likely, these variations (and the outlier for Subject 5 with single integrator CE dynamics) point to a negligible contribution of the near-viewpoint response. Consequently, it is impossible to obtain a meaningful estimate of  $\tau_n$ .

## VI. DISCUSSION

In this paper, we explained how HCs use preview for control in manual tracking tasks with various CE dynamics, using both offline model analyses and experimental data. The hypothesized performance improvement with preview, in accordance with [9]–[11], was confirmed, predominantly in target tracking (H.I). Offline model simulations predicted the attained performance improvement remarkably well, especially considering that no remnant was included, and no parameter interactions were investigated. As hypothesized (H.II), disturbance-rejection behavior and performance were similar with and without preview.

Fitting the model to the experimental data allowed us to peek inside the black-box of human control, decomposing their behavior into several characteristic responses and physically interpretable parameters. Thereby, we confirmed that subjects respond to the target farther ahead in tasks with higher-order CE dynamics (as suggested before in [14]), to compensate for the CE's larger phase lag (confirming H.III). The adopted far-viewpoint location was anticipated quite accurately with the

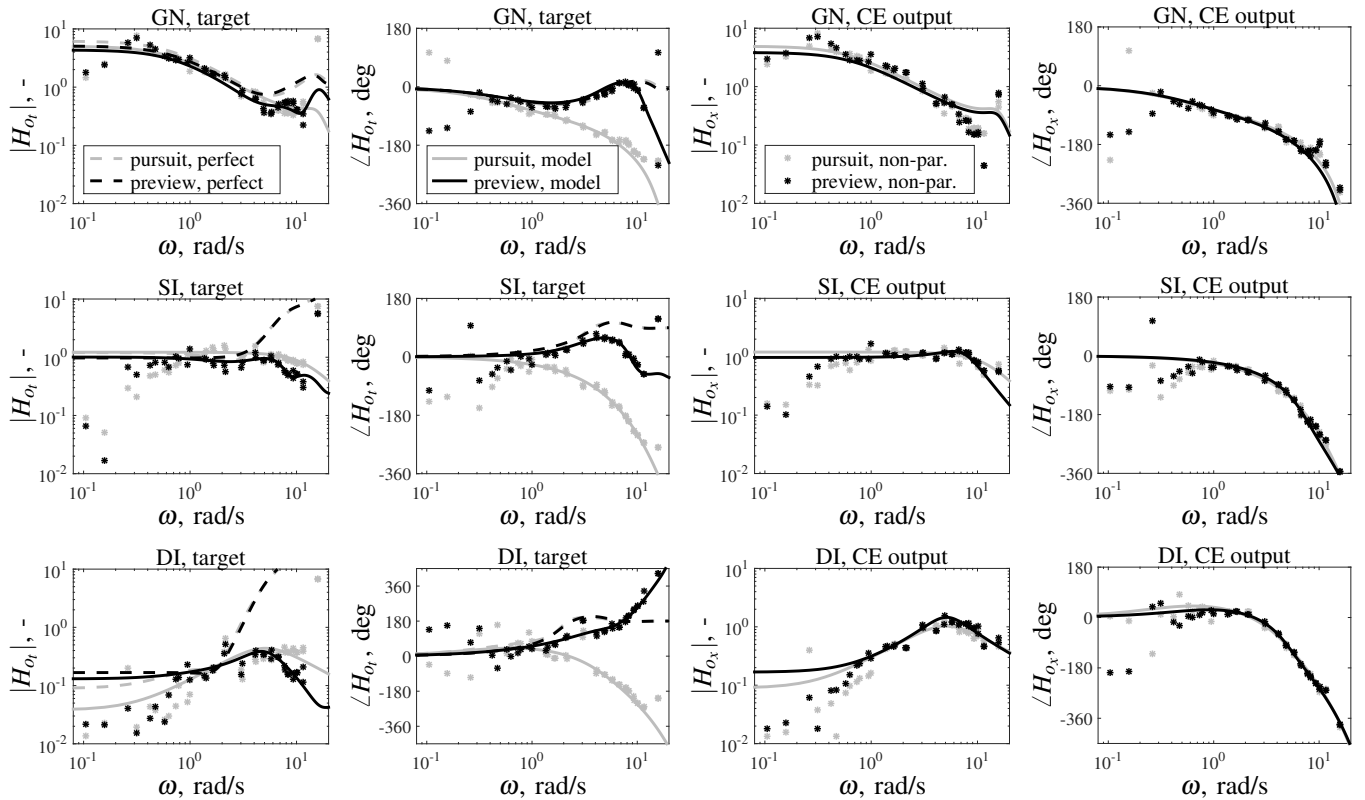


Fig. 12. Bode plots of the target and CE output dynamics: non-parametric estimates, model fits, and perfect target-tracking dynamics; single-subject data.

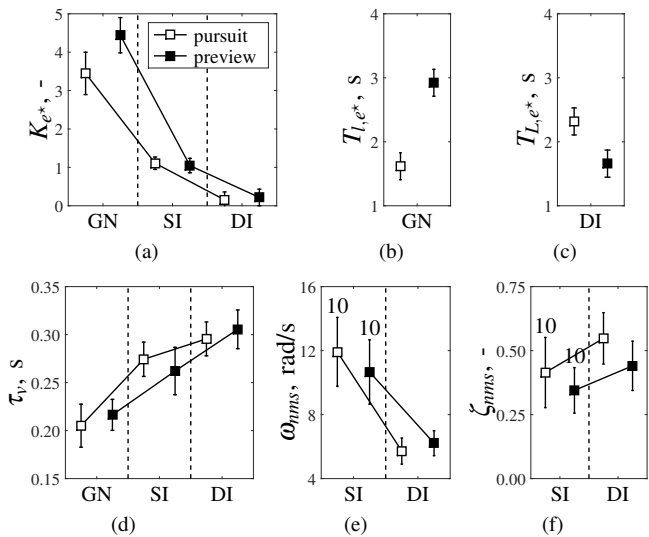


Fig. 13. Estimated internal-error response (a-c) and physical limitation (d-f) parameters. For GN and SI the NMS could be estimated for 0 and 10 subjects, respectively.

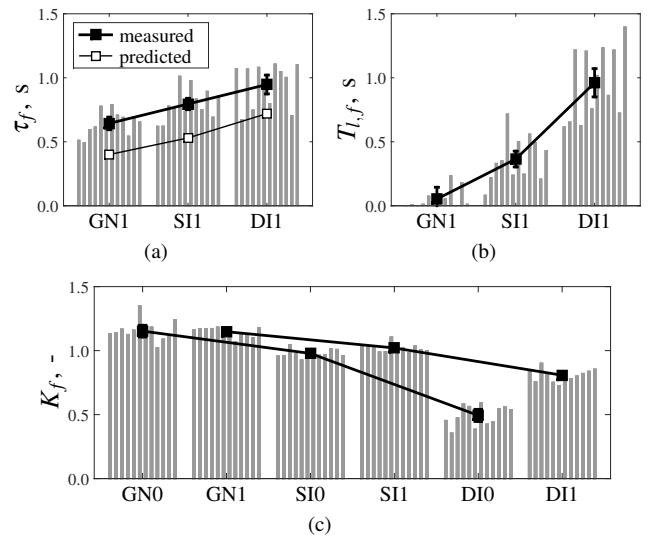


Fig. 14. Estimated far-viewpoint parameters: negative delay  $\tau_f$  (a), lag time-constant  $T_{l,f}$  (b), and gain  $K_f$  (c). Gray bars represent the individual subjects.

offline model simulations, establishing the model's capability to predict HC behavior.

At the highest input frequencies, HCs cannot invert the CE dynamics, as required to attain perfect target-tracking, with just their far-viewpoint response. The role of the additive near-viewpoint response is to better match the perfect target-tracking dynamics at these high frequencies, and to further increase the target crossover frequency. The hypothesized

low but non-zero values for  $K_n$  (H.IV) were found in the experiment for most subjects, but these were not always supported by a clearly visible near-viewpoint response in the corresponding non-parametric target response  $H_{oi}(j\omega)$ . The estimated value of  $K_n$  is a poor indicator for the presence of a near-viewpoint response, hence we cannot confidently confirm H.IV. The near-viewpoint response varies substantially between subjects, likely because it can yield only a marginal performance benefit, at the cost of substantially more control

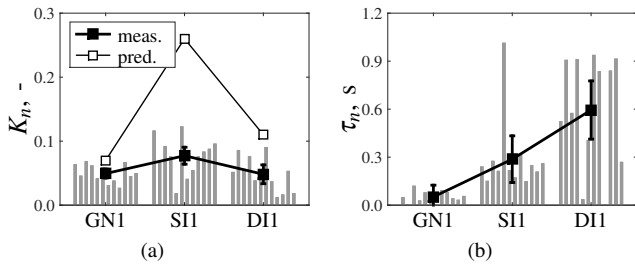


Fig. 15. Estimated near-viewpoint parameters: gain  $K_n$  (a), and negative delay  $\tau_n$  (b). Gray bars represent the individual subjects.

activity. For adequate task performance, the far-viewpoint response is much more important than the near-viewpoint response.

To better illustrate human adaptation between pursuit and preview tracking tasks, and to the CE dynamics, we now propose a first set of verbal adjustment rules. 1) Similar as in compensatory tracking tasks [2], HCs equalize their internal error response  $H_{o_e}(j\omega)$  to the given CE dynamics such that their combination exhibits integrator-like dynamics. 2) In pursuit and preview tasks, HCs apply feedforward control by adapting the relative target-tracking/CE-stabilization priority through  $K_f$ , with more emphasis on target tracking (higher  $K_f$ ) in tasks with lower-order CEs. 3) In preview tasks, HCs anticipate the target signal's changes by basing their "pursuit" response on the far viewpoint  $\tau_f$  s ahead, which is positioned farther ahead for higher-order CEs. Hereby, the response phase (hence performance) improves at lower frequencies but deteriorates at higher frequencies. 4) HCs filter these high frequencies from the previewed target signal by adapting  $T_{l,f}$ ; they filter away more high frequencies (higher  $T_{l,f}$ ) for higher-order CEs. 5) Optionally, performance can be enhanced slightly more by also tracking the target signal's high frequencies with an additive, parallel near-viewpoint response, which ideally resembles the inverse of the CE dynamics. With a near-viewpoint response, HCs sacrifice some phase margin in favor of a higher crossover frequency. These proposed adjustment rules can be refined and extended by quantifying HC adaptation to other task variables, like the preview time and the forcing functions' characteristics.

## VII. CONCLUSION

In this paper, we explained how humans use preview for control in tracking tasks with various controlled element dynamics. We presented offline analyses with a quasi-linear model and results from a human-in-the-loop experiment, to established the roles of the human's near- and far-viewpoint responses. Preview allows humans cancel their own and the controlled element's lags, up to relatively high frequencies, by basing their far-viewpoint, pursuit response on the target signal ahead; this requires no additional control activity. The optional open-loop near-viewpoint response helps to synchronize the output with the target signal at higher frequencies, but at the cost of substantially more control activity. Target-tracking performance improves primarily due to the far-viewpoint response mechanism, while the benefit from the near-viewpoint

response is small. The adopted control-theoretic approach provided unique quantitative insights into human control adaptation in preview tasks, which can explain human behavior observed in other preview control tasks, like driving.

## REFERENCES

- [1] L. R. Young, "On Adaptive Manual Control," *IEEE Trans. Man-Machine Systems*, vol. 10, no. 4, pp. 292–331, Dec. 1969.
- [2] D. T. McRuer and H. R. Jex, "A Review of Quasi-Linear Pilot Models," *IEEE Trans. Human Factors in Electronics*, vol. 8, no. 3, pp. 231–249, May 1967.
- [3] D. T. McRuer, D. Graham, E. S. Krendel, and W. J. Reisener, "Human Pilot Dynamics in Compensatory Systems, Theory Models and Experiments with Controlled Element and Forcing Function Variations," Air Force Flight Dynamics Laboratory, Wright-Patterson Air Force Base, OH, Tech. Rep. AFFDL-TR-65-15, 1965.
- [4] W. W. Wierwille, J. R. Knight, and G. A. Gagne, "An Experimental Study of Human Operator Models and Closed-Loop Analysis Methods for High-Speed Automobile Driving," *IEEE Trans. Human Factors in Electronics*, vol. 8, no. 3, pp. 187–201, Sep. 1967.
- [5] C. C. MacAdam, "Application of an Optimal Preview Control for Simulation of Closed-Loop Automobile Driving," *IEEE Trans. Systems, Man, and Cybernetics*, vol. 11, no. 6, pp. 393–399, Jun. 1981.
- [6] S. D. Keen and D. J. Cole, "Bias-Free Identification of a Linear Model-Predictive Steering Controller From Measured Driver Steering Behavior," *IEEE Trans. Systems, Man, and Cybernetics - Part B: Cybernetics*, vol. 42, no. 2, pp. 434–443, Apr. 2012.
- [7] A. E. Patla and S. Rietdyk, "Visual Control of Limb Trajectory over Obstacles during Locomotion: Effect of Obstacle Height and Width," *Gait & Posture*, vol. 1, pp. 45–60, 1993.
- [8] R. A. Scheidt and C. Ghez, "Separate Adaptive Mechanisms for Controlling Trajectory and Final Position in Reaching," *Journal Neurophysiology*, vol. 98, pp. 3600–3613, 2007.
- [9] L. D. Reid and N. H. Drewell, "A Pilot Model for Tracking with Preview," in *Proc. 8th Ann. Conf. Manual Control*, Ann Arbor, MI, 1972, pp. 191–204.
- [10] M. Tomizuka and D. E. Whitney, "The Preview Control Problem with Application to Man-Machine System Analysis," in *Proc. 9th Ann. Conf. Manual Control*, Cambridge, MA, 1973, pp. 429–441.
- [11] K. Ito and M. Ito, "Tracking Behavior of Human Operators in Preview Control Systems," *Electrical Eng. in Japan*, vol. 95, no. 1, pp. 120–127, 1975, (Transl.: D.K. Ronbunshi, Vol. 95C, No. 2, Feb. 1975, pp 30-36).
- [12] T. B. Sheridan, "Three Models of Preview Control," *IEEE Trans. Human Factors in Electronics*, vol. 7, no. 2, pp. 91–102, Jun. 1966.
- [13] R. A. Hess, "A Model-Based Theory for Analyzing Human Control Behavior," in *Advances in Man-Machine Research*, W. B. Rouse, Ed. JAI Press, 1985, vol. 2, pp. 129–176.
- [14] K. van der El, D. M. Pool, H. J. Damveld, M. M. van Paassen, and M. Mulder, "An Empirical Human Controller Model for Preview Tracking Tasks," *IEEE Trans. on Cybernetics*, vol. 46, no. 11, pp. 2609–2621, Nov. 2016.
- [15] R. J. Wasicko, D. T. McRuer, and R. E. Magdaleno, "Human Pilot Dynamic Response in Single-loop Systems with Compensatory and Pursuit Displays," Air Force Flight Dynamics Laboratory, Wright-Patterson Air Force Base, OH, Tech. Rep. AFFDL-TR-66-137, 1966.
- [16] R. A. Hess, "Pursuit Tracking and Higher Levels of Skill Development in the Human Pilot," *IEEE Trans. Systems, Man, and Cybernetics*, vol. 11, no. 4, pp. 262–273, Apr. 1981.
- [17] M. C. Vos, D. M. Pool, H. J. Damveld, M. M. van Paassen, and M. Mulder, "Identification of Multimodal Control Behavior in Pursuit Tracking Tasks," in *Proc. 2014 IEEE Int. Conf. Systems, Man, and Cybernetics*, San Diego, CA, 2014, pp. 69–74.
- [18] E. S. Krendel and D. T. McRuer, "A Servomechanics Approach to Skill Development," *Journal of the Franklin Institute*, vol. 269, no. 1, pp. 24–42, Jan. 1960.
- [19] E. Donges, "A Two-Level Model of Driver Steering Behavior," *Human Factors*, vol. 20, no. 6, pp. 691–707, Dec. 1978.
- [20] L. Saleh, P. Chevrel, F. Claveau, J. F. Lafay, and F. Mars, "Shared Steering Control Between a Driver and an Automation: Stability in the Presence of Driver Behavior Uncertainty," *IEEE Trans. on Intelligent Transportation Systems*, vol. 14, no. 2, pp. 974–983, 2013.
- [21] H. R. Jex, R. E. Magdaleno, and A. M. Junker, "Roll Tracking Effects of G-vector Tilt and Various Types of Motion Washout," in *Proc. 14th Ann. Conf. on Manual Control*, 1978, pp. 463–502.

- [22] M. M. van Paassen and M. Mulder, "Identification of Human Operator Control Behaviour in Multiple-Loop Tracking Tasks," in *Proc. 7th IFAC/IFIP/IFORS/IEA Symposium on Analysis, Design and Evaluation of Man-Machine Systems*, Kyoto, Japan, 1998, pp. 515–520.
- [23] R. L. Stapleford, D. T. McRuer, and R. E. Magdaleno, "Pilot Describing Function Measurements in a Multiloop Task," *IEEE Trans. Human Factors in Electronics*, vol. 8, no. 2, pp. 113–125, Jun. 1967.
- [24] R. W. Allen and H. R. Jex, "An Experimental Investigation of Compensatory and Pursuit Tracking Displays with Rate and Acceleration Control Dynamics and a Disturbance Input," NASA, Washington, D.C., NASA Contractor Report NASA CR-1082, 1968.
- [25] G. C. Beerens, H. J. Damveld, M. Mulder, M. M. van Paassen, and J. C. van der Vaart, "Investigation into Crossover Regression in Compensatory Manual Tracking Tasks," *Journal of Guidance, Control, and Dynamics*, vol. 32, no. 5, pp. 1429–1445, Sep.–Oct. 2009.
- [26] V. A. Laurens, D. M. Pool, H. J. Damveld, M. M. van Paassen, and M. Mulder, "Effects of Controlled Element Dynamics on Human Feed-forward Behavior in Ramp-Tracking Tasks," *IEEE Trans. Cybernetics*, vol. 45, no. 2, pp. 253–265, Feb. 2015.



**Max Mulder** (M'14) received the M.Sc. degree and Ph.D. degree (*cum laude*) in aerospace engineering from TU Delft, The Netherlands, in 1992 and 1999, respectively, for his work on the cybernetics of tunnel-in-the-sky displays. He is currently Full Professor and Head of the section Control and Simulation, Aerospace Engineering, TU Delft. His research interests include cybernetics and its use in modeling human perception and performance, and cognitive systems engineering and its application in the design of "ecological" interfaces.



**Kasper van der El** (S'15) received the M.Sc. degree in aerospace engineering (*cum laude*) from TU Delft, The Netherlands, in 2013, for his research on manual control behavior in preview tracking tasks. He is currently pursuing the Ph.D. degree with the section Control and Simulation, Aerospace Engineering, TU Delft. His Ph.D. research focuses on measuring and modeling human manual control behavior in general control tasks with preview. His current research interests include cybernetics, mathematical modeling, and system identification and parameter estimation.



and optimization techniques.

**Daan M. Pool** (M'09) received the M.Sc. and Ph.D. degrees (*cum laude*) from TU Delft, The Netherlands, in 2007 and 2012, respectively. His Ph.D. research focused on the development of an objective method for optimization of flight simulator motion cueing fidelity based on measurements of pilot control behavior. He is currently an Assistant Professor with the section Control and Simulation, Aerospace Engineering, TU Delft. His research interests include cybernetics, manual vehicle control, simulator-based training, and mathematical modeling, identification,



**Marinus (René) M. van Paassen** (M'08, SM'15) received the M.Sc. and Ph.D. degrees from TU Delft, The Netherlands, in 1988 and 1994, respectively, for his studies on the role of the neuromuscular system of the pilot's arm in manual control.

He is currently an Associate Professor at the section Control and Simulation, Aerospace Engineering, TU Delft, working on human-machine interaction and aircraft simulation. His work on human-machine interaction ranges from studies of perceptual processes and manual control to complex cognitive systems. In the latter field, he applies cognitive systems engineering analysis (abstraction hierarchy and multilevel flow modeling) and ecological interface design to the work domain of vehicle control.

Dr. van Paassen is an Associate Editor of the IEEE TRANSACTIONS ON HUMAN-MACHINE SYSTEMS.